Final Report: Atomic Resonance Radiation Energetics Investigation as a Diagnostic Method for Non-Equilibrium Hypervelocity Flows

Scott A. Meyer
Daniel Bershader
Stanford University
Stanford, CA

Surendra P. Sharma
George S. Deiwert
NASA Ames Research Center
Moffett Field, California

Funding for the support of this study has been allocated by the NASA-Ames Research Center, Moffett Field, California, under Interchange No. NCA2-723.

Presented by
D. Bershader
4/15/96

Abstract

This is the final report for NCA2-723. Absorption measurements with a tunable vacuum ultraviolet light source have been proposed as a concentration diagnostic for atomic oxygen, and the viability of this technique is assessed in light of recent measurements. The instrumentation, as well as initial calibration measurements, have been reported previously. We report here additional calibration measurements performed to study the resonance broadening line shape for atomic oxygen. The application of this diagnostic is evaluated by considering the range of suitable test conditions and requirements, and by identifying issues that remain to be addressed.

Introduction

Spectral absorption and emission lines are caused by transitions between discrete energy levels of the atom. When observed under low resolution, the lines can appear very sharp, but with higher resolution the lines exhibit a finite width due to line broadening. The line shape plays an important role in radiative transport because the amount of light absorbed at a given wavelength depends not only on the strength of the transition, but also on the line shape. In a gas that is strongly radiating, emission lines may become so intense that some of the emitted light is re-absorbed. The gas is then "optically thick" at this wavelength, and the degree of re-absorption in the line depends on the line shape. The line shape can be predicted reliably when dominated by Doppler or lifetime broadening, but collisional broadening is more difficult to evaluate.

We report collisional broadening measurements for atomic oxygen lines under conditions dominated by resonance interactions, *i.e.* collisions with other oxygen atoms. This work is motivated by an interest in far wing absorption measurements of atomic oxygen at 130 nm as a potential concentration diagnostic for reacting flows. We previously described instrumentation for vacuum ultraviolet absorption measurements in a shock tube, and reported initial measurements at an oxygen atom density of $9\text{x}10^{17}$ cm^{-3}.[1, 2] We have subsequently used this instrumentation to make improved measurements at a density of $3\text{x}10^{17}$ cm^{-3}, and from these measurements have deduced an empirical broadening coefficient for resonance interaction. Previous studies of resonance broadening focused on noble gases and metallic vapors.[3, 4, 5] To our knowledge, these are the first broadening measurements of dissociated species such as hydrogen, nitrogen, or oxygen.

Theory

In this section, impact and static models are applied to atomic oxygen. Spin-orbit coupling produces a splitting of the ^{3}P ground state into three sub-levels, each denoted by their j-values. The resulting triplet consists of lines at 130.21685, 130.48576, and 130.60286 nm.[6] Relevant transition properties are shown in Table 1.[7] Note that the absorption cross sections in the table must be used with the number density in the absorbing state, not the total atomic number density.

The interaction potential between the two atoms, $V(r)$, can be expanded in a power series in $1/r$,[8] and the effect on the radiation field determined by perturbation theory. At interatomic separations, r, which are large relative to the atomic size, the leading term can provide a fair approximation to the potential. As the separation is decreased, higher order terms are required. Inclusion of more realistic interaction potentials is an obvious avenue to improve line broadening predictions.

When a single term of the expansion is sufficient, the interaction leads to a shift in frequency given by the general form $\Delta\omega = C_p/r^p$. The value of p depends on the type of interaction. When the atom of interest (A) and the perturber (B) are of the same type, then a resonance exists between the two particles. The resulting state is a superposition of degenerate states in which either A or B is excited, and the interaction potential is given by a dipole-dipole interaction. The interaction arises from a quantum-mechanical resonance which exists between two like atoms in which the atoms are exchanging "virtual" photons. This interaction occurs for collisions in which the perturber (B) is in an energy level connected by a dipole-allowed transition to either the upper or lower energy level of the transition. Resonance broadening is commonly only important for those lines whose upper or lower levels are dipole-connected to the ground state because, in many cases, most perturbers are in the ground state. The following sections describe two limiting cases for line broadening theories: the impact approximation, which is valid near the center of the line, and the quasi-static approximation, which is valid in the line wing regions.

In the impact approximation, the atom is assumed to oscillate at the transition frequency ω_o until a collision with a perturber. The impact causes a phase shift in the oscillation, and the subsequent oscillation is not coherent with the original wavetrain. Resonance broadening of the lines can be calculated with the impact approximation.[9] The resulting line shape is a Lorentzian with the full width at half maximum (FWHM)

$$\omega_R = 4\pi\sqrt{\frac{7}{3}}\frac{e^2 f_a}{8\pi\varepsilon_o m\omega_o}\sum_{j=0}^{2}\sqrt{\frac{g_a}{g_e}}n_j \qquad (1)$$

where the lower (absorbing) level is denoted a, and the upper (emitting) level is denoted e. This equation differs in two ways from the original reference. The width is multiplied by two to give the FWHM, and the units for the

electron charge have been changed from electrostatic units. In this model the effect of relative collision velocity cancels out, so the linewidth is independent of temperature.

A summation is required to account for collisions with atoms in each of the three different j-levels of the ground state.[1] The role of collisions with atoms in different j in absorption can be understood by first considering their role in emission. The emission process begins with an excited state atom in $^3S^o$. If this atom collides with a ground state atom in j=2, for example, the collision produces a resonance interaction since a dipole transition is allowed between these two states. Despite the interaction, however, the atom can still decay into any of the three j-levels. In the reverse process, then, an atom can begin in the j=1 level, for example, and transition into $^3S^o$. If a collision with a j=2 atom occurs during this process, a resonance interaction will occur and the absorption line is broadened. In wavenumber units, the width is

$$\bar{\nu}_R = 4.84x10^{-20}\sum_{j=0}^{2}\sqrt{\frac{g_a}{g_e}}n_j \; cm^3cm^{-1} \tag{2}$$

For atomic oxygen, the summation can be determined approximately by assuming that the relative populations in the j-levels are given by the degeneracies of the levels. This ratio is exact in the limit of very high temperatures, and is a good approximation at temperatures high enough to dissociate oxygen. With this approximation, the Lorentzian width for resonance broadening is

$$\bar{\nu}_R \approx 5.39x10^{-20}\, n_l cm^3 cm^{-1} \tag{3}$$

The resonance linewidth thus depends only on the number density of colliding atoms in the lower state, n_l. The lower state is the ^3P ground state, so for many cases, n_l is nearly equal to the total number of oxygen atoms.

In the quasi-static approximation, nearby perturbers shift the energy levels of the atom so that the transition frequency is different from that of an unperturbed atom. The distribution of perturbed frequencies for different atoms forms the line profile. The model is developed by first assuming that the positions of the perturbers, and not the velocities, determine the perturbation in the line frequency. The shift in energy levels caused by any configuration of perturbers is calculated and the probability distribution of possible configurations is then used to assign probabilities to each shift. The resulting line profile maps out the probability of any given shift. Making the "nearest neighbor" approximation and assuming an inverse power law with p=3 for resonance broadening yields the quasi-static line shape[10]

$$_{QS}\phi_R(\Delta\bar{\nu}) = \frac{|\Delta\bar{\nu}_o|}{\Delta\bar{\nu}^2}\exp\left[-\left|\frac{\Delta\bar{\nu}_o}{\Delta\bar{\nu}}\right|\right] \approx \frac{|\Delta\bar{\nu}_o|}{\Delta\bar{\nu}^2} \tag{4}$$

The width parameter is the shift due to a perturber at the mean distance between particles, and depends on the interaction constant, C_3. In circular frequency units (rad/sec), the interaction constant is

$$C_3 = \zeta\frac{e^2 f_a}{8\pi\varepsilon_o m\omega_o} \tag{5}$$

The value of ζ is on the order of one, and depends on the orientation of the dipole moments relative to the line between radiator and perturber. In addition, both positive and negative frequency shifts are possible, depending also on the orientation. An estimate of ζ can be obtained from the result for hydrogen.[10] The resulting width parameter (*not* the FWHM) is

$$\Delta\bar{\nu}_o = \frac{1}{72\pi^3 c}\lambda^3 n_l A_{130.49} = 7.04x10^{-21}\, n_l \; cm^3cm^{-1} \tag{6}$$

As in the impact approximation, the width depends on the transition probability and on the number density of atoms in the lower (*i.e.*, ^3P) level.

Validity of the impact and quasi-static models depends on two requirements. The impact approximation is valid when (1) the collision duration is much shorter than the time interval between collisions, and (2) the line shape is calculated at frequency separations from the line center for which the inverse of the separation is much longer than the duration of a collision. Consequently, impact theory is valid near the center of the line and is subject to the following criterion[9]

$$|\bar{\nu} - \bar{\nu}_o| \ll \frac{1}{2\pi c}\left(\frac{g_e}{g_a}\right)^{1/4}\left(\frac{4\pi\varepsilon_o m\omega_o}{e^2 f_a}\right)^{1/2}\left(\frac{kT}{M}\right)^{3/4} \tag{7}$$

The region of applicability depends only on the (translational) temperature and on the given transition. At 6000 K, the term on the right hand side is 13 cm^{-1}. Experimental line shape measurements are made over a frequency range of approximately 2 - 60 cm^{-1}. In this intermediate region, neither the impact nor the quasi-static theories are expected to be strictly valid.

Although the impact and quasi-static models are very different, line shapes calculated with the two models are nearly the same in the intermediate region. For example, the line shape for a number density in the ^3P state, n_l, of $9x10^{17}$ cm^3, can be calculated in the impact approximation with Eqn. 3, and for the quasi-static model with Eqns. 4 and 6. Results are plotted in Fig. 1 as a function of the distance from the center of the line. The Lorentzian profile is almost constant near the line center, then exhibits an inverse quadratic dependence on frequency. The quasi-static profile behaves differently near the line center, but it also has an inverse quadratic dependence in the wings. However, both of these curves have been extrapolated far beyond the regions in which they are valid. According to Eqn. 7, the impact approximation is valid at frequencies much less than 13 cm^{-1} away from the line center. At very large separations, the assumption that the broadening collisions are "instantaneous" fails. On the other hand, the quasi-static theory is valid for frequencies much more than 13 cm^{-1} away. Near the center of the line, the assumption that broadening is independent of the colliding particle motion breaks down. Neither theory is strictly valid in the intermediate region where the absorption measurements are made; however, the two models give virtually the same results. The figure shows that the two profiles have the same functional form and agree to within about 20% in this region.

The absorption profiles are calculated with Beer's Law, and the lines due to each individual *j*-level are included explicitly in the calculation. All three lines have the same absorption cross-section, which is listed in Table 1, along with frequencies of the three line centers. Number density in each *j*-level is given by a Boltzmann distribution at 6100 K, determined from the energy levels and degeneracies also listed in Table 1. The path length is the internal diameter of the shock tube, 10 cm.

Variation of the absorption with frequency is calculated from the line shape function. A common method for combining various broadening mechanisms is convolution into a Voigt profile.[10] To do this, however, the resonance line shape must be modeled with a Lorentzian profile, and this requires the following approximation:

The impact approximation, which produces a Lorentzian, is invalid in the intermediate line wing region. However, the quasi-static model which is applicable in the far wings has the same frequency dependence and is only 20% lower. Therefore, the resonance line shape is modeled with a Lorentzian profile.

Experiment

Shock tube test conditions: The lineshape is determined empirically by measuring transmission over a range of wavelengths where the test conditions are known. Molecular oxygen is dissociated in the Electric Arc-driven Shock Tube (EAST) Facility at NASA-Ames Research Center.[11] A shock speed of 6.8 km/sec is selected because it provides an atomic oxygen sample in thermodynamic equilibrium with a minimum of interfering species, especially molecular oxygen and free electrons.. The first measurements were made with an initial pressure of 1.00 torr oxygen.[1] By reducing the initial pressure to 0.30 torr, we reduce the widths of the absorption lines and can measure the background absorption level directly.

Flow in the shock tube is characterized with shock speed and emission measurements, described briefly here and more extensively in Refs. 1 and 2. Composition of the test gas is determined from the shock speed assuming equilibrium. Measured shock speed is corrected for attenuation with an approximate model in which laboratory time

is converted into particle time to determine the upstream location where the gas was shocked. Effective shock speed, at that location, is determined from measured shock attenuation.

Progress of the dissociation reaction is evaluated with emission measurements. Time-resolved traces show an initial spike due to the nonequilibrium overshoot, which is consistent with nonequilibrium calculations performed with NONEQ.[12] Absorption is measured after this nonequilibrium region passes, 6.4 μsec after shock arrival. In the first experiments at high density, temperature was deduced by comparing synthetic emission spectra to absolute-intensity calibrated spectra recorded with a gatable OMA. Gas composition was calculated assuming chemical equilibrium.[1]

The second measurements are at a lower density (0.3 torr driven tube pressure). At this test condition reaction rates are slower, but more direct measurements are available to characterize the test gas. Atomic density is again deduced from shock speed measurements. The number density is lower, so background absorption can be measured directly in the region between the atomic lines. Flow characterization is therefore more empirical; calculations are used only to deduce atomic density and to infer an upper limit on Stark broadening.

Absorption is measured at the same delay time behind the incident shock. Time-resolved ultraviolet emission recorded with a CsTe photomultiplier shows that the nonequilibrium overshoot ends well before the laser pulse. At this test condition virtually all of the O_2 dissociates, so that small deviations from chemical equilibrium will not affect the atomic number density. Background absorption is measured at several delay times to determine the optimum time to measure the line profile. This absorption, presumably due to O_2, decreases quickly behind the shock. Internal delays in the laser and the finite width of the port plug windows prevent measurements directly behind the shock; however, the earliest possible measurement shows that the absorption disappears quickly. Excessive corrections for background absorption are not required.

Equilibrium conditions behind the shock wave are calculated with the EQGAS code, which solves the one-dimensional shock wave equations for a real gas. Equilibrium constants are derived from partition functions calculated for molecular and atomic species from spectroscopic constants. Calculated test gas compositions are shown in Table 2 for the nominal shock speed, and for shock speeds one standard deviation higher and lower than nominal.

Baseline absorption is measured directly in the lower density measurements, so an independent determination of O_2 concentration is not required. Analysis of the data does not require a strong statement about thermochemical equilibrium to determine the O_2 density. The equilibrium composition for this test condition is virtually complete dissociation, so the atom concentration is within a few percent of the equilibrium value long before equilibrium is reached. Since most electrons are produced by O^+, the electron density is also unlikely to be higher than its equilibrium value. Thus, analysis of the data requires only that the test gas be nearly in equilibrium. Time resolved emission traces indicate that this condition is reached within a few μsec after shock arrival.

VUV instrumentation: Figure 2 is a schematic of the instrumentation. Light from a tunable, pulsed ArF laser is focused into a Raman shifter to produce vacuum ultraviolet light. The Raman shifter is filled with hydrogen at 350 torr and 77 K, and generates linearly polarized beams at numerous wavelengths. One of these overlaps the O line at 130.49 nm.[13] This beam is separated from the others by a pair of 30° MgF_2 prisms. Incident and transmitted intensities are measured by KBr photomultipliers which are insensitive to residual light at 193 nm. Measurements with a CaF_2 window whose transmission is 50% at 130 nm verify that the photomultiplier tubes operate in a linear range. Although absolute intensity of the probe beam was not measured, comparison to Ref. 13 suggests a value in the neighborhood of 10^{-6} J. Several O_2 Schumann-Runge absorption lines overlap the ArF tuning range, and these lines are used for wavelength calibration. The low density measurements require more accurate wavelength calibration, provided by a microwave discharge cell between the shock tube and the photomultiplier for measuring transmitted intensity. Atomic oxygen is generated by adding NO to a stream of N atoms generated in the discharge. Laser-induced fluorescence scans in the cell provide absolute wavelength calibration, and indicate that the linewidth of the Raman-shifted beam is 0.9 cm^{-1}. This linewidth is sufficiently small to resolve the absorption profiles of atomic oxygen.

Results and Discussion

Empirical lineshape: The theoretical and empirical absorption profiles are shown in Figs. 3 and 4. The high density measurements have been reported previously, and are reproduced here for completeness. The three lines overlap in the line wings and the peak measured transmission is less than 50%. Measurements in the two tuning bands indicated in the figure probe the absorption profile around the j=1 transition at 130.49 nm. Vertical error bars are produced by uncertainty in the reference intensity, and the horizontal error bars by the linewidth of the probe laser and by uncertainties in the line position. Absorption by the j=1 transition is clearly shown by the data, but the

background absorption level cannot be measured between the lines. The gap in the tuning band prevents measurements in the spectral region where the absorption profile varies most rapidly.

The new measurements are at lower density to alleviate some difficulties with the previous measurements and to evaluate the effect of number density on linewidth. Relative contributions from the various broadening mechanisms are similar, so these measurements are also dominated by resonance broadening. The lines are narrower so overlap is reduced substantially, and background transmission is measured between the lines. The profile for j=1 is contained in the available tuning bands and is not expected to vary substantially in the tuning gap. As a result of the narrower line, measurements are made on both sides of the line center. No asymmetry is observed within the uncertainty of the measurement.

The theoretical absorption profiles are calculated for each line with Beer's Law, and the line shape functions are calculated from theoretical linewidths. Doppler, lifetime, and Stark linewidths calculations are described in Ref. 1. The resonance width is calculated with the impact model, using Eqn. 3. Theoretical curves compare favorably with the data. The empirical width is deduced by fitting absorption profiles to the data with the Lorentzian width as a free parameter. Resonance broadening produces most of the Lorentzian width, so the empirical linewidth for resonance broadening is found from the empirical Lorentzian width by subtracting corrections for the other broadening mechanisms.

The fitting procedure includes an offset for background absorption. Absorption by undissociated O_2 in the core flow and recombined O_2 in the boundary layer are the only mechanisms expected at this temperature. In the high density case this background is estimated from emission measurements and absorption cross-sections. Calculated O_2 density in the core flow is listed in Table 2. Thickness of the velocity boundary layer is estimated to be 0.83 mm.[14] This correlation is for air, not for oxygen, but comparison between flat plate calculations for equilibrium and completely dissociated oxygen suggest that chemical reactions introduce about a 20% error in the estimate of the velocity boundary layer thickness. The concentration profile of O_2 is estimated from flat plate calculations for dissociating oxygen, with the distance from the leading edge selected to reproduce the velocity boundary layer thickness.

Absorption by O_2 is estimated from high-temperature cross-section data.[15] Unfortunately, the value of the cross-section at 6000 K and its variation with temperature are not known as precisely as the value at 300 K. The temperature variation estimated by Evans and Schexnayder is based on approximations which are now known to be flawed, and subsequent analysis has focused on temperatures below 1000 K. Therefore, the experimental value at 6400 K is adopted, and various approximate models of the temperature variation are evaluated to estimate boundary layer absorption. Core flow absorption is estimated at 5±5%, and boundary layer absorption at 5±5%. In consideration of the approximations involved, total background is estimated at 10±10%. Empirical fits to the high density data are shown for baseline absorption of 0 and 20%. Not shown are fits assuming a larger baseline than the estimated values; however, such fits are visibly inferior to those shown. A Lorentzian width of 0.057 cm^{-1} is deduced for this test condition. Corrections of 0.0034 cm^{-1} and 0.0010 cm^{-1} for lifetime and Stark broadening, respectively, yield a self-broadening width of 0.052 cm^{-1}, FWHM.

Baseline for the low density measurements is included as a parameter in the curve fitting, and corrections for adjacent lines, while still included, are much smaller. Least squares curve fits are carried out with the Lorentzian width and background absorption as free parameters. Curve fits are performed first on the transmission data, and then on the logarithm of transmission (optical depth). The two fits provide different relative weightings to the data points, with the first placing more emphasis on the highest transmission points. The second fit places more emphasis on the points where absorption is strongest, and is more appropriate where uncertainty is proportional to the measured transmission at each point. The resulting linewidths differ by only 6%; the average value is 0.0160 cm^{-1} with a background absorption of 8%, and is shown in Fig. 4. After subtracting corrections of 0.0034 cm^{-1} and 0.0002 cm^{-1} for lifetime and Stark broadening, a self-broadening width of 0.0124 cm^{-1}, FWHM, is obtained for this condition.

The measured linewidths are compared to theoretical models in Fig. 5. The measured linewidths and the impact model agree very well. The quasi-static model is calculated with results for hydrogen, and so is only approximate. Discrepancies between theory and measurements are within the estimated experimental error. A resonance broadening coefficient can be deduced from the data, assuming a linear dependence on atomic oxygen number density. The empirical linewidth (Lorentzian FWHM) is

$$_{Expt.}\overline{\nu}_{Resonance} = 4.9x10^{-20} n_l cm^{-1} cm^3 \tag{8}$$

where n_l is the number density of atoms in the ^3P state. The broadening coefficient predicted with the impact model (Eqn. 3) agrees well with this value.

Experimental error sources: Imperfections in transmission measurements and uncertainties in data analysis lead to errors in the empirical linewidths. The important measurement uncertainties include uncertainty in reference intensity, probe beam wavelength and linewidth, and spectral purity of the probe. These produce the vertical and horizontal error bars on the transmission data. Uncertainties in the data analysis include broadband absorption, other broadening mechanisms, and atomic number density.

Uncertainty in the reference intensity is the largest uncertainty in the transmission measurements. Despite several experimental modifications, this error source was not eliminated. The magnitude of the error is determined by evaluating the scatter in calibration measurements performed before each shot. Statistical analysis of 100 shots taken before each shot yield standard deviations of 7-13%. Although the average value of the calibration factor between reference and transmitted tubes is known accurately, a single shot transmission measurement is limited by the magnitude of this scatter. This statistical error is the source of the vertical error bars in the transmission measurements.

Wavelength calibration and beam linewidth are the sources of the horizontal error bars, which are not a significant error source in the experiment. Beam linewidth and wavelength are measured with a microwave flow cell, and the measured width of 0.9 cm^{-1} provides sufficient resolution for this experiment.

Spectral purity of the probe beam requires narrowband light at the desired wavelength and rejection of other Raman orders and stray light. Spectral measurements with a scanning monochrometer demonstrated that stray light is eliminated, but the Q-branch at 130 nm consisted of both narrowband and broadband components. During absorption measurements, however, the probe beam is completely attenuated when tuned to the center of the line. Based on locking efficiency measurements, the broadband component could produce an apparent transmission of roughly 10%. This is not observed, however, indicating that no broadband or stray light contaminates the measurements. The discrepancy between preliminary spectral scans and absorption measurements is probably the result of two differences between the measurements. First, the hydrogen cell pressure is reduced for the absorption measurements to reduce the VUV intensity and to assure linear operation of the PMT's. If broadband conversion is less efficient than narrowband conversion, this will enhance the fraction of narrowband light. Second, the dynamic range of the digitizer (TEK 2440) is reduced by about 10% when operated at its highest sample rate, which is used in these measurements. This limitation was not immediately apparent because the digitized signals are slightly distorted, but not clipped, and this affected the spectral scan data. However, the absorption measurements are all made within the available dynamic range and are not affected.

Several other potential measurement errors exist which are not expected to be significant. Broadband emission from the test gas is observed only in the high density case, where it appears as a slowly varying baseline beneath the VUV probe pulse. The probe pulse is time-resolved and background emission can be easily subtracted out. Atomic transitions can be saturated with an intense probe beam, but this is less likely when collisional broadening, rather than Doppler broadening, is dominant. Strong saturation of the transitions would produce measurable transmission at line center, which is not observed. Beam steering by the test gas can potentially deviate the beam from the detector. Although the index of refraction is high near the transitions, gradients in atomic concentration should be relatively weak. The limiting aperture at the detector is wider than the shock tube window to minimize this effect, but no measurements are performed to quantify it.

The number of absorbers depends on the total number of atoms and on the *fraction* of atoms in the absorbing state, $2p^4\ ^3P_1$. Uncertainties in atomic number density depend on both statistical and systematic errors. Atomic concentrations in the shock tube are reproducible to within ±9%, 2σ. Two systematic error sources are expected. First, boundary layer growth reduces the effective absorption pathlength, but only by 1-2%. Second, atomic number density is deduced from corrected shock speed measurements. The correction is about 10% and the systematic error is expected to be significantly less than this correction. The *fraction* of atoms in $2p^4\ ^3P_1$ depends on electronic temperature, and at 6000 K, the temperature dependence is extremely weak. A non-Boltzmann distribution, if present, primarily affects excited states which account for only a small fraction of all atoms; the $2p^4\ ^3P_1$ population fraction should not be appreciably affected.

Deduction of the linewidth also depends on the total absorption cross-section or line strength. The ^3P-$^3S^o$ transitions are strongly dipole-allowed, so reliable transition probabilities have been calculated which are in good agreement with experiment.[16] Uncertainty in the absorption cross-section is estimated at ±10%. This error source affects the measured broadening coefficient, but in practice does not affect calculations made with it. The cross-section is a physical constant, not an experimental parameter, so uncertainties in the cross section do not affect the *product* of the cross section and line shape function found in Beer's Law.

Background absorption by O_2 can be caused by undissociated oxygen in the core flow and recombined oxygen in the boundary layer. The effect of baseline errors on the empirical width has been evaluated analytically and numerically. Taking partial derivatives in Beer's Law shows that the relative error depends on the transmission. At a typical transmission of 50%, a 2% change in baseline produces a 3% change in the apparent Lorentzian width.

Numerical evaluation for the high density case verifies this result, and the uncertainty in the width for this condition is ±15%.

Competing broadening mechanisms must be separated out to deduce the resonance broadening linewidth. In the line wings, Doppler broadening is insignificant, and corrections for other mechanisms are subtracted from the measured line width. Lifetime broadening is independent of thermodynamic properties and can be reliably subtracted out, assuming that the elementary theory is valid in the far line wings. Stark broadening effects are more difficult to calculate. The equation used for Stark broadening by electrons is cited in Ref. 1. Stark broadening by ions is often modeled differently, but in this study it is treated approximately by setting it equal to the electron broadening for lack of a better model. An independent measurement of electron density generally improves the accuracy of Stark corrections. Although electron density was not measured directly, the current test conditions were chosen to minimize the effect of Stark broadening on the measured linewidth.

Mapping out the line profile with a series of single-shot shock tube measurements produces most of the measurement uncertainty through the mechanisms described above. The effect of limited sample size and scatter is difficult to evaluate. However, it can be estimated by considering the statistical variation of the empirical linewidth with the number of measurements. The question, "How much would another data point reduce the uncertainty in linewidth?" can be answered approximately by taking away one of the data points and deducing the linewidth from the remaining points. Repeating this process for all data points produces an estimate of the scatter in the deduced linewidth. This analysis has been performed for the low density case, and the standard deviation in the deduced linewidths is 3.4%. Therefore, *non-systematic*, random errors produce an uncertainty of about 7% (2σ) in the measured linewidth. Systematic errors contribute as well, and the estimated uncertainty in the broadening coefficient is 20-30% (2σ).

Two experimental improvements would reduce uncertainty in the background absorption. First, thoroughly purging the beam paths of oxygen reduces width of the tuning gap, allowing measurements in part of that region. Second, transmission below 10% can be measured more accurately by calibrating with an absorbing filter, such as a thick CaF_2 or MgF_2 window. A higher PMT voltage, and thus larger signals, can be used if the calibrations are performed for 10% transmission instead of 100% transmission.

Comparison to previous work: Resonance broadening has been studied extensively both experimentally and theoretically, although not with oxygen atoms. Previous research has focused on metallic vapors and noble gases because they are experimentally more convenient and theoretically simpler to model. Unlike oxygen, these species are readily obtained as free atoms, and transition wavelengths are in the visible or ultraviolet. Theoretical analysis is also more direct because the oxygen transitions are from a triplet lower state with more fine structure levels to consider. However, it is useful to discuss the present measurements in the context of previous work.

Hydrogen is a particularly simple system with only a single electron. King and Van Vleck[17] evaluated the long-range resonance (or dipole-dipole) interaction between excited and ground state atoms. As the atoms approach each other, they become coupled and take on the character of molecular wavefunctions. Results for an S lower state and a P upper state are especially simple when spin is neglected, and the interaction for various m-values is easy to evaluate. Despite extensive study of this system, experimental verification faces the same obstacles as the current experiment of dissociating a molecular gas and probing a VUV transition. Kielkopf[18] describes proposed experiments using a laser-produced plasma to study Lyman-α radiation, but only preliminary results are given.

Theoretical analyses of hydrogen have been applied to metallic vapors, which are more convenient to study experimentally. Atomic vapors are generated in ovens and the number densities determined from vapor-pressure curves. Niemax and Pichler[3] studied absorption of Na, K, Rb, and Cs at densities that scaled several orders of magnitude. Accuracy of the experiments are limited by knowledge of number density, but high resolution scans can be performed on the static samples. Absorption in the wings generally exhibits a quadratic dependence consistent with quasi-static broadening theory. Deviations from quadratic behavior are found in the far wings. Initially this was attributed to the difference between Σ and Π potential curves,[19] but trends in the data for all alkalis suggest that deviations are produced by distortions of the potentials by avoided crossings. Avoided crossings will occur at interaction energies related to the spacing of the atomic energy levels. For oxygen, this corresponds to energies in the range of about 20-80 cm^{-1}, but the current measurements are not sufficiently numerous or precise to detect such deviations.

Noble gases are also convenient sources of atoms. Resonance broadening affects not only the resonance lines which terminate in the ground state, but also lines whose *lower state is connected to the ground state* by a dipole-allowed transition. Kuhn and Lewis[4] and Hindmarsh and Thomas[5] measured resonance broadening of emission lines in He, Ne, Ar, and Kr. Carefully designed discharges are required to eliminate other broadening mechanisms, but lines whose lower levels connect to the ground state are wider than other lines.

Similar results are expected for oxygen emission lines, so the effects of resonance broadening are also important for transitions other than the VUV triplet studied here. Numerous states are connected to the $2p^4\ ^3P$

ground state by appreciable dipole moments, and transitions terminating in these levels experience resonance broadening. The resonance width is calculated with the dipole moment of the transition to the ground state, not of the transition being considered. For example, the 845 and 437 nm transitions are resonance-broadened because they terminate in $3s\ ^3S^\circ$. On the other hand, the 777 nm triplet terminates in $3s\ ^5S^\circ$, and is not subject to resonance broadening.[20] Differences in Lorenztian widths between these types of lines depends on the ground state O density. In principle, the differences might be measured to deduce O density in a high temperature flowfield, although in practice this may be difficult to implement. Resonance broadening of lines between excited states should certainly be included in radiative transport calculations, especially for lines which become optically thick.

Resonance interactions are studied in a fundamentally different way with level-crossing measurements. Specifically, vapor atoms are optically pumped into excited states with polarized light, allowing selective excitation of specific *m*-sublevels of the excited state.[21] Various mechanisms, including resonance interactions with other atoms, cause transitions to other *m*-sublevels which can be monitored by observing the depolarization of fluorescence emitted from the system. Happer and Saloman[22] studied resonance interactions with lead whose ground state is ^3P. The electron configuration is $6p^2\ ^3P$, and because the outer shell is less than half full, the order of *j*-levels is opposite that of oxygen. Splitting of the "ground state" levels is larger by a factor of 50, so only the $j=0$ level is appreciably populated; collisions with atoms in other *j*-levels are infrequent. Although measurements and theory agree very well in these measurements, direct comparison to oxygen is not possible. However, these measurements address the behavior of individual *m*-levels, providing an alternative approach to evaluating resonance interaction models.

Limitations of current model: The resonance broadening models described earlier are in good agreement with the empirical broadening coefficient for oxygen. This model contains many approximations, however, and the effect of these approximations should be evaluated before extrapolating the broadening calculation to substantially different thermodynamic conditions.

The broadening model determines the functional form of the lineshape (Voigt, Lorentzian, inverse power law, etc.). Limiting cases of impact and quasi-static approximations are assumed in the data analysis, although neither is strictly valid. Approximate validity criteria are available,[9, 23] but the true validity range of these models has yet to be established.[3] Furthermore, the models assume interactions with only the nearest neighbor. Complications introduced by resonance interaction of more than two atoms were outlined by Margenau and Watson,[23] but resonance broadening models generally neglect these interactions which become important at high densities. Finally, the broadening model neglects inelastic collisions. Peach[24] analyzed the behavior of the lineshape function in the region between the impact and quasi-static limits, including the effects of multiple perturbers. The line shape functions, however, are not valid for resonance interactions which are not additive for multiple perturbers.

Numerical analysis can improve line broadening models because approximations made to achieve closed-form solutions are no longer required. One-term approximations to interaction potentials, for example, can be replaced by more realistic models. In early work, King and Van Vleck[17] pointed out the relationship between the potential curve for a diatomic molecule and the interaction potential between two atoms. Resonance interaction dominates at large interatomic separations, but higher order terms in the power series expansion become important at small separations. Effects of these terms manifest themselves as asymmetries and deviations from Lorentzian behavior in the far line wings. In fact, broadening by collisions with similar atoms is sometimes referred to as self-broadening to acknowledge that such interactions are not limited to dipole-dipole resonance forces.

Tremendous strides in computational chemistry have made calculations of interaction potentials very common, especially for air species like O_2. Saxon and Liu[25] report *ab initio* potentials for all combinations of oxygen atoms in the lowest ^3P, ^1D, and ^1S states, including the $^3P + ^3P$ combinations. They subsequently reported similar calculations on several Rydberg states of O_2, including two singlet states arising from the separated atom limit $3s\ ^3S^\circ + ^3P$;[26] however, potentials for all states arising from this configuration are not available. Accuracy of the calculations is not sufficient for detailed broadening calculations, although the authors noted that accuracy was not limited by the state of the art (in 1977). Even without more sophisticated calculations, judicious analysis with these potentials can provide insight into the limitations of the inverse power law potential.

Evaluation of line broadening with molecular potentials requires consideration of many details not explicitly treated in approximate models. For example, transitions are not allowed between all combinations of upper and lower states, but instead depend on transition probabilities between states of various symmetries. Furthermore, these states correlate with different separated atom limits (*i.e.*, $j=2, 1, 0$). In the approximate model, these effects are accounted for by an "empirical" factor in the resonance width. In the separated atom limit, the effect of individual *m*-levels must be determined by explicitly summing over all such levels. Extrapolation of these effects to a pair of interacting atoms is more complicated because angular momenta of the two atoms couple. Transition from the

separated atom limit to molecular states, including the effects of degeneracies, has been described by Chang,[27] although excited states and resonance interactions are not considered.

Diagnostic applications: The original motivation of this work was to develop an optical diagnostic technique to determine the ground state number density of atomic oxygen. In this study, we focused on demonstrating VUV absorption measurements with a tunable laser system and studying the effect of resonance broadening on the absorption line shape. The following section discusses issues related to implementation of the diagnostic, including the applicable range of test conditions and additional technical issues to be resolved.

The appeal of this technique is the ability to measure ground state number density, which can easily be related to the total number density of oxygen atoms. Absorption measurements determine the number density in the j=1 state, which is a function of electronic temperature. At low temperatures, most of atoms are found in the j=2 level. With increasing temperature, the population ratio between the three levels approaches the 5:3:1 ratio of the degeneracies, and the partition function approaches nine. At much higher temperatures, other states become populated and the Boltzmann fraction in the ground state gradually decreases. Over a large range of temperatures where oxygen dissociation is important, the Boltzmann fraction is a weak function of temperature. Specifically, the population fraction in j=1 is within 10% of 3/9 from 1100 to 14000 K.

Absorption measurements with a tunable light source have a larger dynamic range than those made with a fixed-wavelength source. Width of the j=1 (130.49 nm) absorption line is shown in Fig. 5.6 for a range of Lorentzian widths and density-pathlength products. Number density on the y-axis refers to the total atomic oxygen number density and is based on the assumption that the Boltzmann fraction for j=1 is one-third. Calculations assume a Lorenztian shape; Gaussian contributions are neglected, which is approximately valid for the conditions shown on this plot. For lines narrower than those shown, Doppler broadening must be included. The minimum Lorentzian width for which calculations are plotted corresponds to the lifetime linewidth. Absorption linewidths are defined as the full width between 50% transmission points on the j=1 profile. For very wide lines, contributions from the adjacent lines are no longer negligible, and actual widths will be larger than those shown. The applicable range of densities depends on a variety of parameters, but the figure suggests a range of at least 10^{16}-10^{18} cm^{-3} for a 10 cm pathlength. At lower densities, the laser linewidth must be deconvolved from the absorption profile; at higher widths, adjacent lines must be accounted for and direct measurement of background absorption is difficult.

Similar information can be displayed in an alternative style by plotting the atomic oxygen absorption cross-section as a function of laser frequency relative to the j=1 line. Cross-sections are calculated from Voigt profiles to show the large cross-section at the resonance frequencies, where Doppler broadening is dominant. These cross-sections are relative to total atomic oxygen number density. Results are shown for conditions with only lifetime broadening and for lifetime broadening plus a collisional width ten times larger than the lifetime width. Results are shown in Fig. 7 for Doppler widths and population distributions at 6000 K.

The broadening coefficient for collisions with other oxygen atoms is deduced from measurements in this work, but widths for other colliders must also be known. The Stark interaction is relatively strong, so Stark broadening by electrons is significant for relatively low densities of electrons. Resonance widths are calculated from the empirical broadening coefficient reported here. Extrapolation of this result assumes that a Lorentzian profile is a fair prediction of the actual line shape. Van der Waals broadening caused by collisions with other neutral particles is not included in the figure. For this transition, the dipole moment is relatively large, so van der Waals interactions should be weaker than the resonance interaction. For a given collider density, broadening by a foreign gas should be much smaller than that due to resonance broadening. Sohns and Kock[28] report a van der Waals interaction constant, C_6, of 6.50×10^{-38} m^6/sec for collisions with argon atoms. If this value is assumed to express the interaction energy in units of rad/sec, it predicts an interaction of 5400 cm^{-1} (0.7 eV) at a separation of 20 Å, which seems high. Other results in the paper are presented in wavelength units, however, so this interpretation may not be correct. Without further experimental data, van der Waals widths can only be estimated from theoretical results.

Broadband absorption is a major potential source of spectral interference. Continuum absorption can be important for a highly ionized test gas, or for one with molecular species that absorb strongly. Vacuum ultraviolet absorption by molecular oxygen is very strong. The photodissociation continuum at room temperature passes through a minimum near 130 nm. Nevertheless, this absorption is still strong, and some experimental evidence indicates that it increases at higher temperatures. In Fig. 7, continuum absorption coefficients for room temperature and 6400 K are included for reference, although the high temperature is subject to a large uncertainty.[2] On resonance, atomic absorption is tremendously stronger than the photodissociation continuum. When the optical depth on resonance is extremely large, as in the current measurements, the photodissociation continuum is stronger than relevant portions of the atomic profile. Atomic absorption measurements are only possible where dissociation is virtually complete. A baseline measurement is a valuable way to correct for any background absorption, but this is difficult when the lines begin to merge together. Alternatively, a secondary source can measure the background just outside the triplet in the region near 129.5 nm. The photodissociation continuum due to Schumann-Runge

contains structure in this whole spectral region, and interpretation of the signal may be somewhat ambiguous. With test conditions such as those encountered in Case A, however, this information may be useful to place an upper limit on the background absorption.

Application of VUV diagnostics in large-scale facilities can lead to several practical difficulties.[2] This system must meet the requirements for high-vacuum and cryogenic operation with high-intensity UV and VUV light. System cleanliness is crucial to prevent oil contamination of optics, since contaminants are burned in by the laser beam, and contaminants in the hydrogen contribute to phase-mismatch as well as VUV absorption and condensation on cold optics. Careful mechanical design of the Raman cell is also required to maintain seals with repeated thermal cycling.[29] However, vacuum, cryogenic, and VUV crystal technology are sufficiently mature that much of the necessary equipment is commercially available. In single-shot applications, shot-to-shot variation of Raman-shifter output can also lead to difficulties in selecting gains for detectors and data acquisition. Individually, all of these complications are surmountable. However, they can complicate efforts to coordinate VUV measurements with facility operations.

Conclusions

We have measured the absorption lineshape of atomic oxygen in the VUV and compared the results to available theories of resonance broadening. Theories for the two limiting cases (impact and quasi-static) give nearly equivalent results in the intermediate line wing region. These theories compare favorably with the experimental measurements when the number density of perturbers is taken as the total population in the ^3P ground state. However, neither theory is strictly valid at the experimental conditions. Comparison to resonance broadening measurements in noble gases and metallic vapors illustrate the limitations of the these models, especially in the far wing region. These limitations should be evaluated for atomic oxygen before extrapolating these results to other conditions. Our work demonstrates that a tunable VUV laser source can extend the range of atomic resonance absorption spectroscopy (ARAS) to substantially higher number densities, although additional spectroscopic data is required.

References

[1]Meyer, S. A., Sharma, S. P., Bershader, D., Whiting, E. E., Exberger, R. J., and Gilmore, J. O., "Absorption Line Shape of Oxygen at 130 nm With a Raman-shifted Laser," AIAA Journal, in press.

[2]Meyer, S. A., "Vacuum Ultraviolet Absorption Measurements of Atomic Oxygen in a Shock Tube," PhD Thesis, Stanford University, 1995.

[3]Niemax, K., and Pichler, G., "New aspects in the self-broadening of alkali resonance lines," J. Phys. B: Atom. Molec. Phys., Vol. 8, No. 2, pp. 179-184, 1975.

[4]Kuhn, H. G. and Lewis, E. L., "Resonance Broadening of Spectral Lines," in Polarisation Matiére et Rayonnement, pp. 341-356. Presses Universitaires de France, Paris, France, 1969.

[5]Hindmarsh, W. R. and Thomas, K. A., "Collision Broadening in the Argon Spectrum," Proc. Phys. Soc., A 77, pp. 1193-96, 1961.

[6]Moore, C. E., "Tables of spectra of hydrogen, carbon, nitrogen, and oxygen atoms and ions," pp. 204, 212, CRC Press, Boca Raton, Florida, 1993.

[7]Hibbert, A., Biémont, E., Godefroid, M., and Vaeck, N., "E1 Transitions of astrophysical interest in neutral oxygen," J. Phys. B: At. Mol. Opt. Phys., Vol. 24, pp. 3943-3958, 1991.

[8]Margenau, H. and Kestner, N. R., Theory of Intermolecular Forces, 2nd ed. Chapter 2, Pergamon Press, New York, 1971.

[9]Ali, A. W., and Griem, H. R., "Theory of Resonance Broadening of Spectral Lines by Atom-Atom Impacts," Phys. Rev., Vol. 140, No., 4A, pp. A1044-1049, Nov. 1965.

[10]Traving, G., "Interpretation of Line Broadening and Shift" in Plasma Diagnostics," ed. Lochte-Holtgreven, W., Wiley Interscience Division, John Wiley and Sons, New York, 1968.

[11]Sharma, S. P., Park, C., and Dannenberg, R. E., "Operating Characteristics of a 60 cm and a 10 cm Electric Arc-driven Shock Tube," AIAA-88-0142, 26th Aerospace Sciences Meeting, Reno, NV, Jan. 11-14, 1988.

[12]Sharma, S. P., and Whiting, E. E., "Modeling of Nonequilibrium Radiation Phenomena: An Assessment," AIAA paper 94-0253, Reno, NV, Jan. 1994.

[13]Döbele, H. F., Hörl, M., Röwekamp, M., and Reimann, B., "Detection of Atomic Oxygen by Laser-Induced Fluorescence Spectroscopy at 130 nm," Appl. Phys. B., Vol. 39, pp. 91-95, 1986.

[14]Mirels, H., "Correlation Formulas for Laminar Shock Tube Boundary Layer," Phys. Fluids, Vol. 9, No. 7, pp. 1265-1272, July, 1966.

[15]Evans, J. S., and Schexnayder, C. J. Jr., "An Investigation of the Effect of High Temperature on the Schumann-Runge Ultraviolet Absorption Continuum of Oxygen," NASA Technical Report R-92, 1961.
[16]Jenkins, D. B., "Oscillator Strength of the 130 nm OI Triplet," J. Quant. Spectrosc. Radiat. Transfer, Vol. 34, No. 1, pp. 55-58, 1985
[17]King, G. W. and Van Vleck, J. H., "Dipole-Dipole Resonance Forces," Phys. Rev., Vol. 55, pp. 1165-72, June 1939.
[18]Kielkopf, J., "The Lyman-alpha Wing," Spectral Line Shapes, Vol. 7, Proc. Eleventh International Conference, Carry le Rouet, France, June, 1992.
[19]Niemax, K., and Pichler, G., "Asymmetric self-broadening of Cs principal lines," J. Phys. B: Atom. Molec. Phys., Vol. 7, No. 10, pp. 1204-13, 1974.
[20]Chang, H. A., Baer, D. S., and Hanson, R. K., "Semiconductor Laser Diagnostics of Atomic Oxygen for Hypersonic Flowfield Measurements," AIAA 93-0628, 31st Aerospace Sciences Meeting, Reno, NV, Jan. 1993.
[21]Kastler, A., "Optical Methods For the Study of Radio-Frequency Resonances," Physics Today, pp. 34-41, Sept. 1967.
[22]Happer, W. and Saloman, "Resonant Collision Broadening of the $(6s26p7s)^3P_o^1$ State in Lead," Phys. Rev., Vol. 160, No. 1, pp. 23-34, Aug. 1967.
[23]Margenau, H. and Watson, W. W., "Pressure Effects on Spectral Lines," Rev. Mod. Phys., Vol. 8, pp. 22-53, Jan. 1936.
[24]Peach 1984
[25]Saxon, R. P. and Liu, B., "*Ab initio* configuration intertaction study of the valence states of O_2," J. Chem. Phys., Vol. 67, No. 12, pp. 5432-41, Dec. 1977.
[26]Saxon, R. P. and Liu, B., "*Ab initio* configuration intertaction study of the Rydberg states of O_2," J. Chem. Phys., Vol. 73, No. 2, pp. 870-880, July 1980.
[27]Chang, T. Y., "Moderately Long-Range Interatomic Forces," Rev. Mod. Phys., Vol. 39, No. 4, pp. 911-942, Oct. 1967.
[28]Sohns, E. and Kock, M., "Plasma Diagnostics Based On Self-reversed Lines - II. Application to Nitrogen, Carbon, and Oxygen Arc Measurements in the Vacuum Ultraviolet," J. Quant. Spectrosc. Radiat. Transfer, Vol. 47, No. 5, pp. 335-343, 1992.
[29]Faris, G. W. and Dyer, M. J., "Raman-shifting ArF excimer laser radiation for vacuum-ultraviolet multiphoton spectroscopy," J. Opt. Soc. Am. B, Vol. 10, No. 12, pp. 2273-86, Dec. 1993.

Table 1. Characteristics of the atomic oxygen triplet at 130 nm

λ, nm	130.21685	130.48576	130.60286
$\bar{\nu}$, cm^{-1}	76794.978	76636.713	76568.001
E_{lower}, cm^{-1}	0.000	158.265	226.977
j_{lower}	2	1	0
g_{lower}	5	3	1
A, sec^{-1}	$3.55x10^8$	$2.12x10^8$	$0.706x10^8$
σ_o, $cm^2\ cm^{-1}$	$4.80x10^{-14}$	$4.80x10^{-14}$	$4.80x10^{-14}$

Table 2. Shock tube test conditions for Case A (1.0 torr initial pressure) and for Case B (0.3 torr initial pressure)

	Case A			Case B		
Speed, km/sec	6.83-0.16	6.83	6.83+0.16	6.74-0.10	6.74	6.74+0.10
Temperature, K	5400	6100	6800	5200	5600	6100
O density, cm^{-3}	$9.6x10^{17}$	$9.0x10^{17}$	$8.4x10^{17}$	$3.0x10^{17}$	$2.9x10^{17}$	$2.7x10^{17}$
O_2 density, cm^{-3}	$6x10^{15}$	$2x10^{15}$	$5x10^{14}$	$9x10^{14}$	$3x10^{14}$	$1.5x10^{14}$
e^- density, cm^{-3}	$2x10^{13}$	$7x10^{13}$	$3x10^{14}$	$4x10^{12}$	$1x10^{13}$	$4x10^{13}$

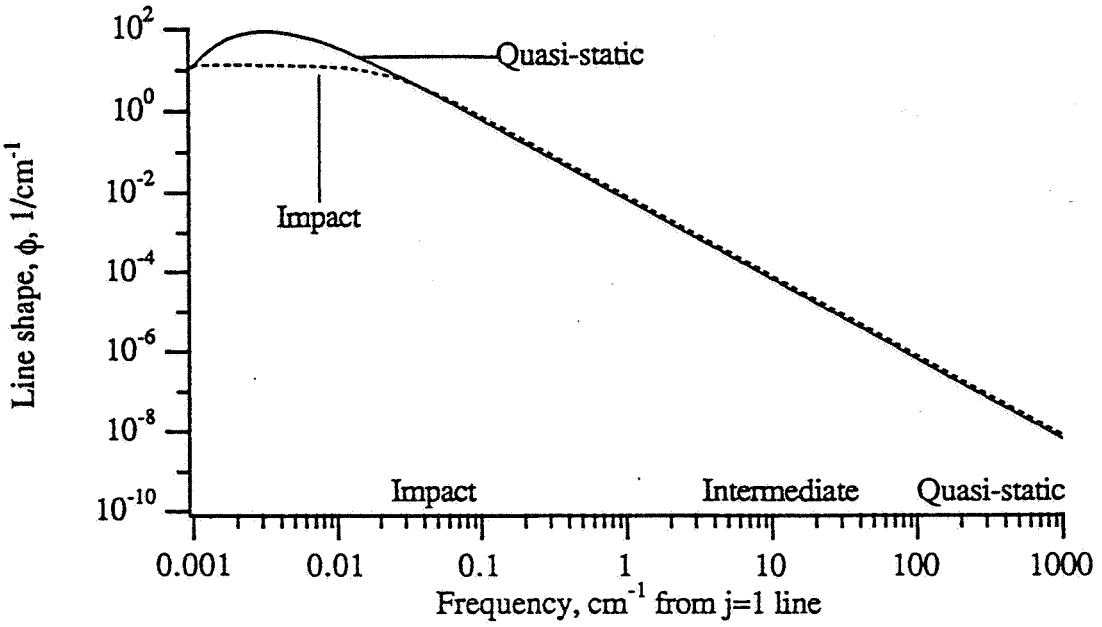

Figure 1. Line shapes for impact and quasi-static models of resonance broadening for the j=1 line at a perturber density of 9×10^{17} cm^{-3}. The impact model is applicable near the center of the line, and the quasi-static in the far wings.

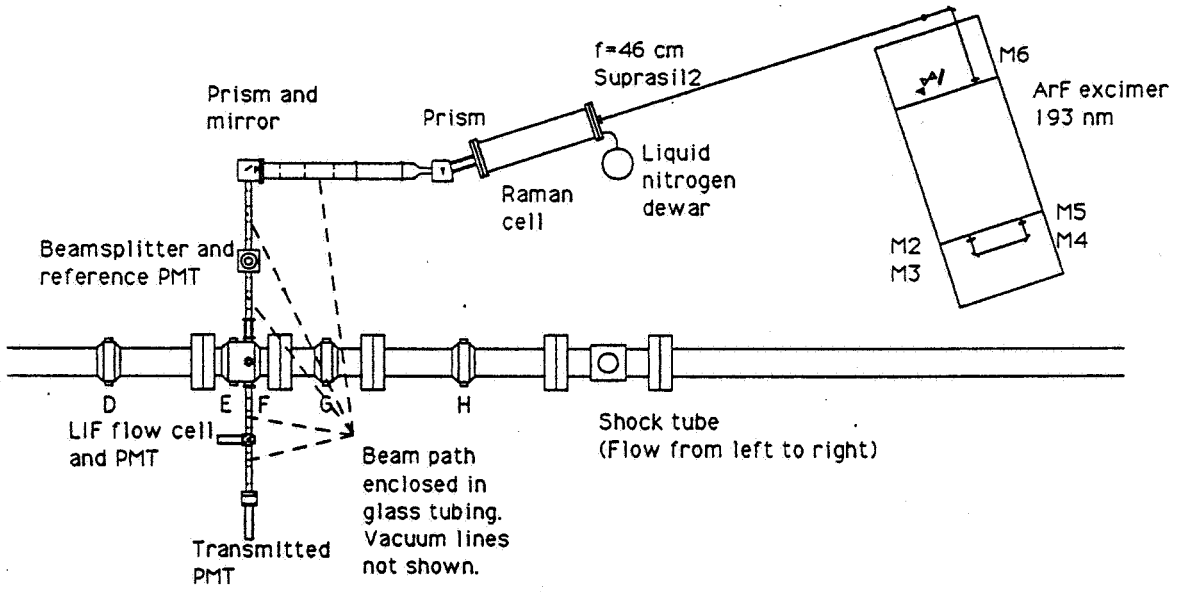

Figure 2. Layout of instrumentation for VUV absorption measurements.

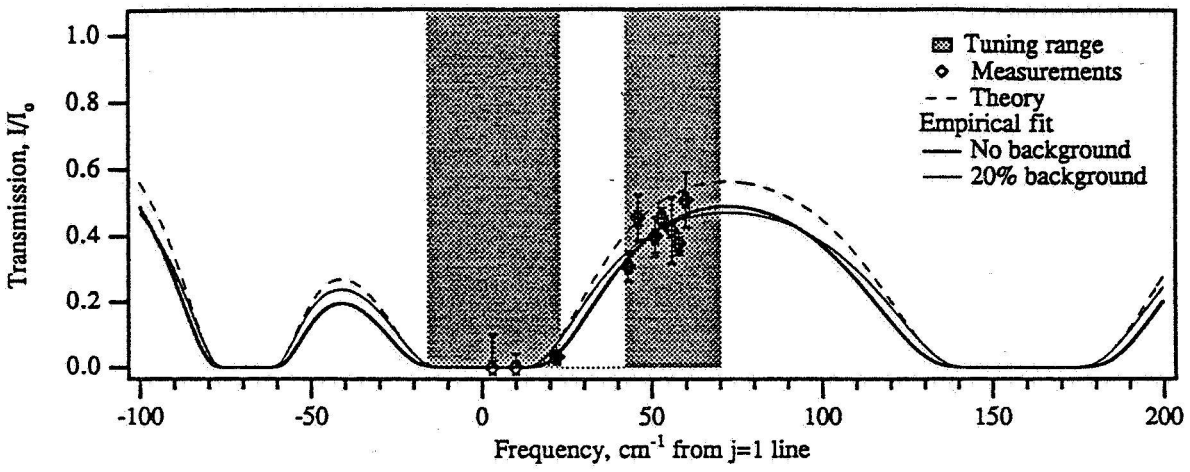

Figure 3 Measured transmission in the region of the j=1 transition (130.49 nm) at 9×10^{17} cm^{-3}.

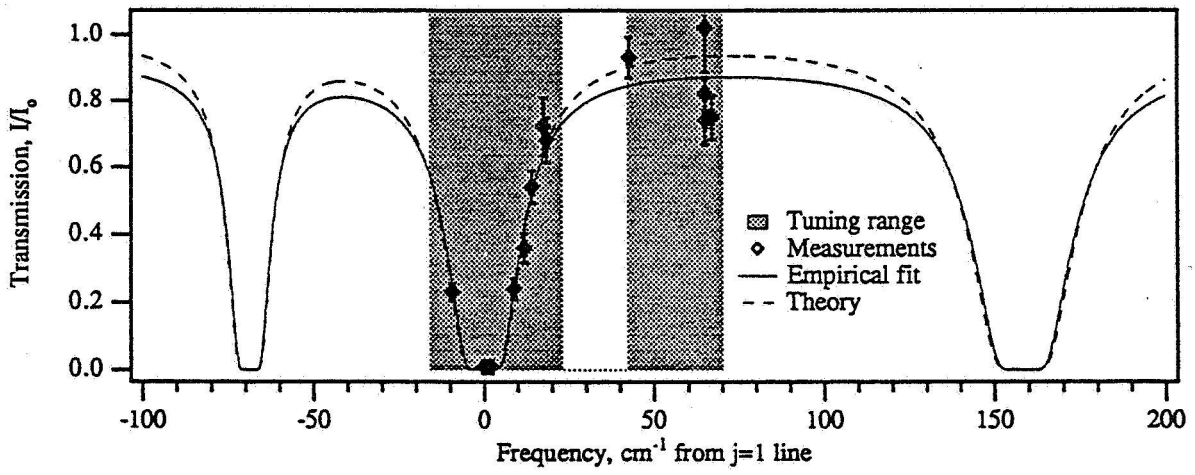

Figure 4 Measured transmission in the region of the j=1 transition (130.49 nm) at 3×10^{17} cm^{-3}.

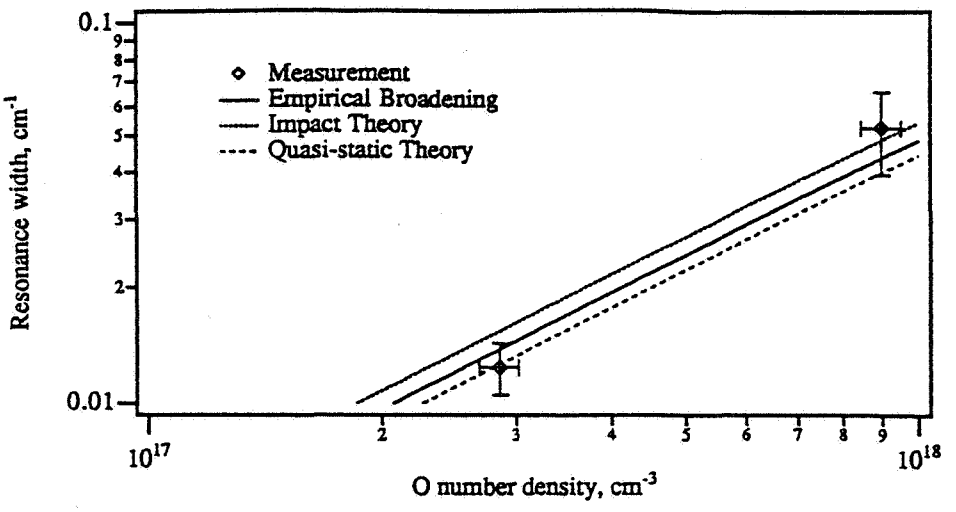

Figure 5. Comparison of linewidths predicted by theory to measured values.

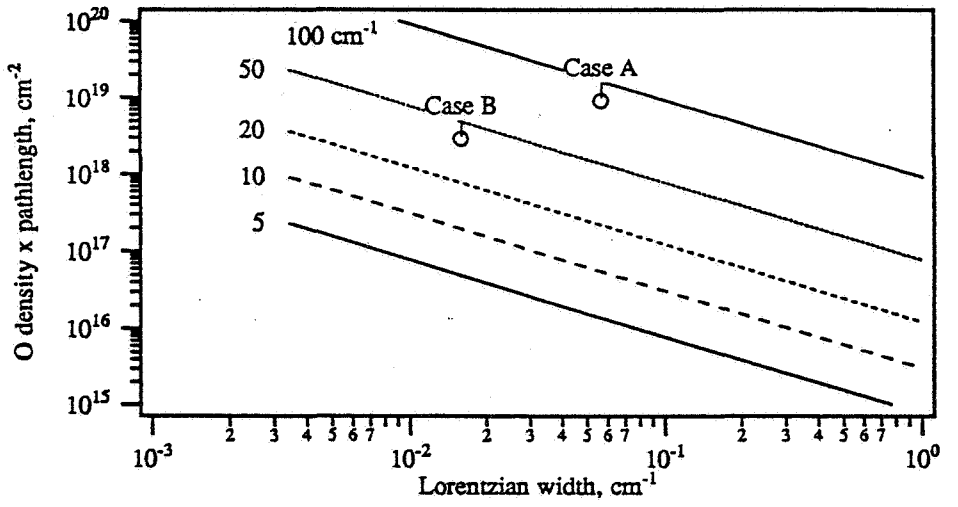

Figure 6. FWHM of absorption line produced as a function of the Lorentzian width and the product of number density and absorption pathlength.

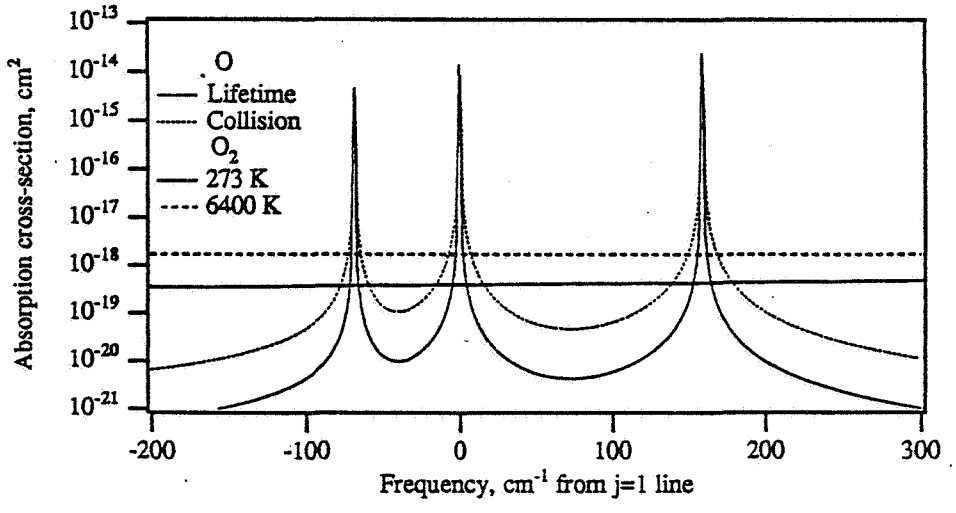

Figure 7. Calculated cross-sections for atomic absorption at 6000 K for two Lorentzian widths. Molecular cross-sections are included for comparison.

Figure 5. Comparison of linewidths predicted by impact and quasi-static theory to measured values.

Figure 7. Calculated cross-sections for atomic absorption at 6000 K with Lorentzian width given by (1) only lifetime broadening and (2) with lifetime broadening plus a collisional width ten times larger. Molecular cross-sections are shown for comparison.

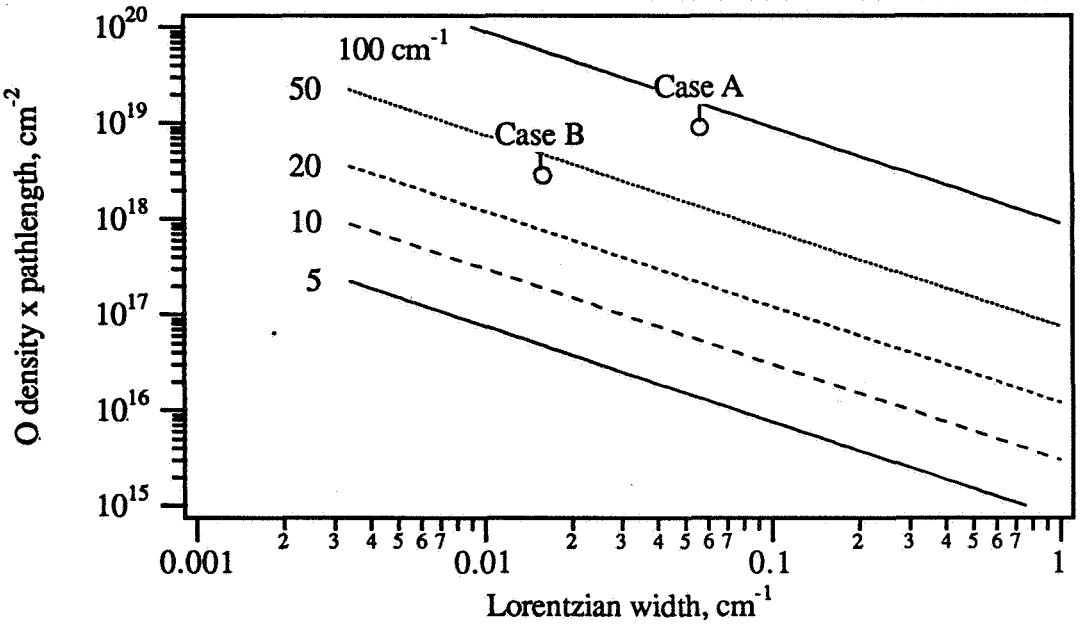

Figure 6. Full width at half maximum of absorption line produced as a function of the Lorentzian line width and the product of atomic number density and absorption pathlength.